



University of Dundee

Geotechnical seismic isolation based on high-damping polyurethane

Tsang, Hing-Ho; Tran, Duc-Phu; Hung, Wen-Yi; Gad, Emad F.

Published in:
Bulletin of Earthquake Engineering

DOI:
[10.1007/s10518-023-01842-4](https://doi.org/10.1007/s10518-023-01842-4)

Publication date:
2024

Licence:
CC BY

Document Version
Publisher's PDF, also known as Version of record

[Link to publication in Discovery Research Portal](#)

Citation for published version (APA):
Tsang, H.-H., Tran, D.-P., Hung, W.-Y., & Gad, E. F. (2024). Geotechnical seismic isolation based on high-damping polyurethane: centrifuge modelling. *Bulletin of Earthquake Engineering*, 22(4), 2001-2023. <https://doi.org/10.1007/s10518-023-01842-4>

General rights

Copyright and moral rights for the publications made accessible in Discovery Research Portal are retained by the authors and/or other copyright owners and it is a condition of accessing publications that users recognise and abide by the legal requirements associated with these rights.

Take down policy

If you believe that this document breaches copyright please contact us providing details, and we will remove access to the work immediately and investigate your claim.



Geotechnical seismic isolation based on high-damping polyurethane: centrifuge modelling

Hing-Ho Tsang¹ · Duc-Phu Tran¹ · Wen-Yi Hung² · Emad F. Gad¹

Received: 15 September 2023 / Accepted: 8 December 2023 / Published online: 9 January 2024
© The Author(s) 2024

Abstract

Geotechnical seismic isolation (GSI) is a new category of low-damage resilient design methods that are in direct contact with geomaterials and of which the isolation mechanism primarily involves geotechnics. Various materials have been explored for placing around the foundation system in layer form to facilitate the beneficial effects of dynamic soil-foundation-structure interaction, as one of the GSI mechanisms. To reduce the thickness of the GSI foundation layer and to ensure uniformity of its material properties, the use of a thin and homogeneous layer of high-damping polyurethane (HDPU) was investigated in this study via centrifuge modelling. HDPU sheets were installed in three different configurations at the interface between the structural foundation and surrounding soils for realising GSI. It was found that using HDPU for GSI can provide excellent seismic isolation effects in all three configurations. The average rates of structural demand reduction amongst the eight earthquake events ranged from 35 to 80%. A clear correlation between the period-lengthening ratio and the demand reduction percentage can be observed amongst the three GSI configurations. One of the configurations with HDPU around the periphery of the foundation only is particularly suitable for retrofitting existing structures and does not require making changes to the structural systems or architectural features.

Keywords Geotechnical seismic isolation · Retrofit · Polyurethane · Centrifuge · Soil-foundation-structure interaction

1 Introduction

Seismic isolation is considered an ideal approach to achieve resilience because the structure being isolated is expected to suffer minimal damages even in a major earthquake event. This can fulfil the low-damage performance requirement. Amongst newly developed techniques, geotechnical seismic isolation (GSI) is a new category of systems that has attracted a lot of attention partly because they are more cost-effective and convenient to implement without the requirements of advanced knowledge and skills (Tsang 2009). Also, GSI shifts

✉ Hing-Ho Tsang
htsang@swin.edu.au

¹ School of Engineering, Swinburne University of Technology, Melbourne, Australia

² Department of Civil Engineering, National Central University, Taoyuan, Taiwan

the focus from altering the structures to making beneficial use of geomaterials or facilitating the beneficial interaction between the structure and surrounding geomaterials. It can isolate the entire structural system including the foundation.

There are three branches of GSI systems, which are classified based on their isolation mechanisms (Tsang and Pitilakis 2023). The first one is achieved by facilitating the beneficial effects of dynamic soil-foundation-structure interaction in a controlled manner to lengthen the natural period of the system and hence lower the structural demand (e.g. Tsang and Pitilakis 2019, Aloisio et al. 2023, Chiaro et al. 2023). The second is to introduce a sliding mechanism between the structural foundation and surrounding geomaterials to limit the amount of seismic energy that is transmitted onto the structure (e.g. Yegian and Kadakal 2004, Yuan et al. 2021, Banović et al. 2023). The third mechanism is based on vibration scattering or filtering, or various forms of damping, to dissipate seismic energy outside the structure (e.g. Kirtas et al. 2009, Forcellini and Alzabeebee 2023, Somma and Flora 2023).

The most researched material for achieving the first GSI mechanism is mixtures of soil and waste tyre rubber granules, commonly referred to as rubber-soil mixtures, since the concept was proposed by Tsang (2008). The performance of GSI systems based on rubber-soil mixtures has been investigated via analytical and numerical modelling (e.g. Tsang et al. 2012, Pitilakis et al. 2015, Brunet et al. 2016), shaking table testing (Dhanya et al. 2023), centrifuge modelling (Tsang et al. 2021) and field testing (Vratsikidis and Pitilakis 2023). Such systems based on rubber-soil mixtures can also mitigate liquefaction potential, as demonstrated in the studies conducted by Bernal-Sanchez et al. (2023) and Nikitas and Bhattacharya (2023). Other materials that have been explored for achieving the first GSI mechanism include EPS geof foam (Karatzia and Mylonakis 2017), EPS beads (Edinçliler and Yildiz 2023), nylon fibres (Shimamura 2012), and so forth.

Whilst the seismic performance of GSI systems based on various materials has been proven to be promising and the serviceability performance is expected to be satisfactory (Tsang et al. 2023), there is room for optimising the systems and improving their performance. One common concern is related to the uniformity of properties when the GSI layer is made of a mixture of different granular materials. The other concern is the required thickness of such a layer, which may inevitably incur additional costs at the site formation stage. In view of these two concerns, a thin and homogeneous layer of high-damping polyurethane (HDPU) was explored in this study via centrifuge modelling.

2 GSI configurations with polyurethane

Polyurethane (PU) is a polymeric material that is composed of organic units connected by carbamate links. PU can be produced in different forms and states, such as rigid and flexible foams. Foams are the most common form of PU that is used in a large variety of applications including those that involve cushioning and energy absorption. PU foam has also been explored for GSI applications based on injection techniques for scattering seismic waves away from existing structures (Gatto et al. 2023). PU-coated waste tyre rubber, which can be collected from the left-over and cut-out in producing flexible sports surfaces and anti-fatigue mats or tiles, has also been studied (Akhtar and Tsang 2023). Using this to produce rubber-soil mixtures can enhance durability, reduce leaching of harmful substances and improve GSI performance.

The type of PU that was used in this study is a soft, stretchy and viscoelastic solid, which is made of long and flexible segments of polyols with low crosslinking and is created through the reaction of polyols and isocyanates. This can offer the required low modulus, elasticity and high damping for optimal GSI performance. There are various products of this type of HDPU in the market, whilst samples of a registered product called Sorbothane® (www.sorbothane.com), in sheet form of 6 mm thick each, provided for free by an Australian distributor, were used in this study. It is expected to have a long fatigue life and a low creep rate compared to other polymers. Also, it is considered to be highly durable, water-resistant, chemical-resistant and insensitive to a wide temperature range, rendering it an ideal candidate for GSI applications.

The 2011 Tohoku (Japan) Earthquake and Tsunami reminded us of the importance of providing special protection to critical infrastructure, such as power plants and hospitals, in which many sensitive facilities and fragile equipment are installed. The majority of those facilities and equipment are classified as acceleration-sensitive, as their main parts and components are usually made rigid with high strength, whilst the most vulnerable parts are the connections and electronics. The outstanding performance and high robustness of HDPU would make it particularly suitable for protecting such infrastructure from ground shocks and high-acceleration motions.

HDPU can be placed around the structural foundation in different configurations as proposed by Tsang (2023). Three configurations were selected for investigation in this study as shown in the schematic diagrams in Fig. 1. The first one is the ‘original’ configuration with a continuous layer of HDPU being placed around the entire structural foundation as shown in Fig. 1A (denoted by C1). This configuration has been studied extensively and can be regarded as the benchmark case in this study. In the second configuration depicted in Fig. 1B, HDPU is only placed around the periphery of the foundation, whilst the foundation base remains in contact with the existing natural soil (denoted by C2a, following the notation adopted in Tsang 2023). Whilst the first configuration is mainly applicable to new structures, the second one can be used for retrofitting existing structures. Also, extra excavation is not required if it is applied to new constructions and there would be no concern about ground settlements. Lastly, the third configuration involves placing HDPU underneath the structural foundation, whilst a gap is created around its periphery as shown in Fig. 1C (denoted by C4, following the notation adopted in Tsang 2023). Also known as lateral disconnection (Somma et al.

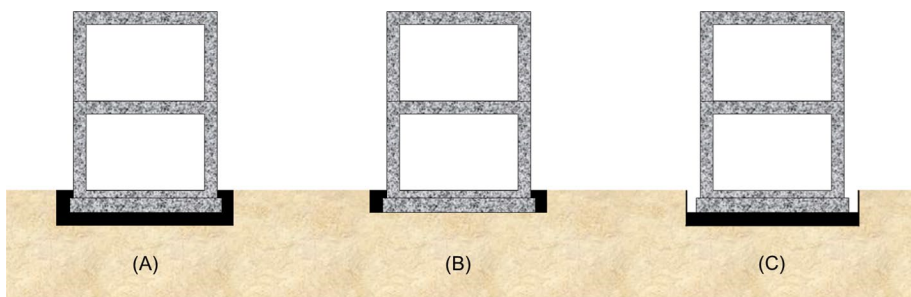


Fig. 1 GSI configurations investigated in this study: **A** HDPU around the entire foundation (C1); **B** HDPU around the periphery of the foundation (C2a); **C** HDPU underneath the foundation with lateral disconnection (C4)

2022), the gap reduces the horizontal and rotational stiffness of the foundation, which can facilitate dynamic soil-foundation-structure interaction in a favourable manner.

3 Centrifuge testing

3.1 Test setup

The testing program was carried out at the Centrifuge Modelling Laboratory at National Central University (NCU) in Taiwan. The dimensions and capacity of the centrifuge apparatus, including the laminar container, along with a couple of photos, can be found in an article previously written by the project team (Tsang et al. 2021). A pair of building frame models as shown in Fig. 2 were adopted in this study. The columns at the four corners of the model provided the required lateral stiffness to the structure that had a fundamental natural frequency of 3.5 Hz, as obtained from free vibration tests. The roof and floor slabs represented the self-weight of the building. GSI-HDPU system was implemented on one model, with the other one serving as a reference case. In this way, direct comparisons of the response behaviours between the two models can be made and the performance of GSI-HDPU systems can be evaluated more conveniently.

Garnier et al. (2007) provide a detailed description of the scaling laws used in this study, which define the relationships between the dimensions and response parameters of the test models and those of the prototype structures. In the tests, a centrifugal acceleration field of 50 g was produced. Hence, the scaling factor for length is 50. Based on this, the prototype building had a height of 5.6 m and a rectangular floor plan measuring 4 m by 5.5 m. It had a shallow embedment depth of 1 m, which included a raft footing of 0.5 m thick. The thickness of the HDPU layer was 0.6 m (i.e. two sheets of HDPU, 6 mm thick each, were used

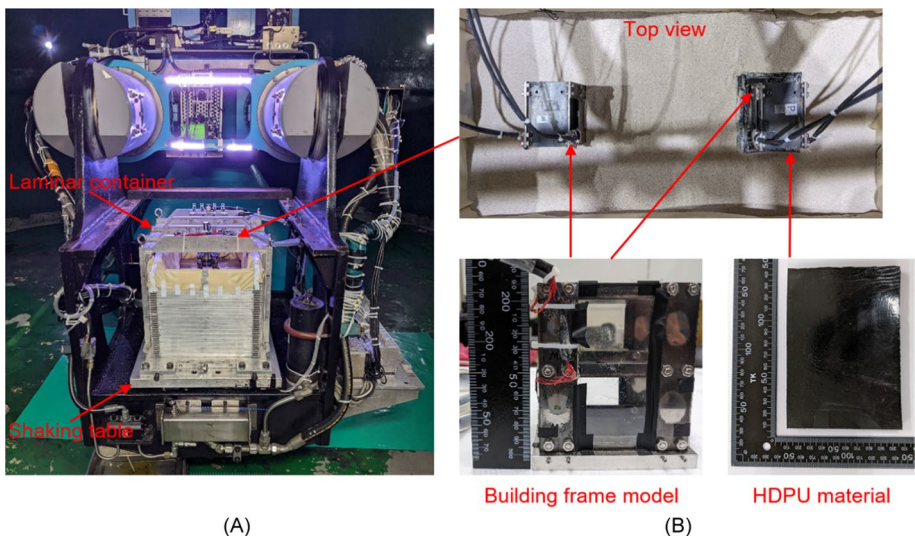


Fig. 2 **A** Centrifuge test setup with a laminar container and shaking table; **B** a pair of building frame models, with one of them using HDPU sheets for creating GSI systems

in the test). All the dimensions and response parameter values presented in this article correspond to the prototype scale, unless stated otherwise.

The natural soil used in the testing was dry quartz sand, with 50% of particles with diameters smaller than (i.e., a median diameter D_{50} of) 0.59 mm and a coefficient of uniformity (C_u) of 1.90, which was classified as poorly graded sand (SP) according to the Unified Soil Classification System (USCS) with less than 5% fines. The maximum and minimum dry density estimated based on ASTM D4253 and ASTM D4254 were 1683 kg/m³ and 1431 kg/m³ respectively. The design density would then be 1599 kg/m³ for a target relative density of 70%. The specific gravity (G_s) of the sand was 2.65 (estimated based on ASTM D854) whilst that of the HDPU material was 1.26 (estimated based on ASTM D792). Hence, the density of the HDPU material was 1260 kg/m³.

The total thickness of the soil in the laminar container was 150 mm, which corresponds to 7.5 m in the prototype scale. The materials were filled layer by layer, each of which was properly compacted to achieve the design density. The fundamental natural frequency of the entire soil layer was estimated to be between 5 and 8 Hz, based on the shear wave velocity values measured for similar materials (Lee et al. 2014), which was then confirmed by the test results reported in Sect. 4.2.4. This was sufficiently distant from the fundamental natural frequencies of the soil-foundation-structure systems that must be lower than 3.5 Hz, which is the natural frequency of the fixed-base frame. Hence, the structural response would not be contaminated by the predominant response of the soil layer.

3.2 Instrumentation

The array of various types of sensors, comprising accelerometers, strain gauges and Linear Variable Differential Transformer (LVDT) displacement sensors, is shown in Fig. 3. Noted that the GSI system on the left-hand side features Configuration C1 as an example. The same array of sensors was deployed in the testing for other GSI configurations.

Accelerometers were placed at each level of the frame models for measuring horizontal acceleration. The acceleration response reduction at the roof (based on A1 and A8) and floor (based on A2 and A9) of the GSI-HDPU systems can be calculated. Horizontal

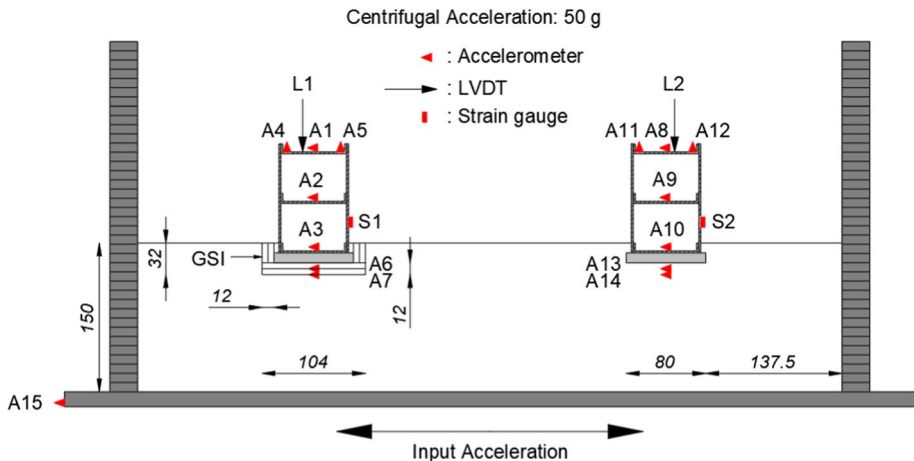


Fig. 3 Centrifuge test set-up with the array of various types of sensors (dimensions in mm)

displacement responses at the roof and floor were not measured or calculated in this study, as the inter-storey drift response was found to have a strong correlation with the horizontal acceleration response in the previous study (Tsang et al. 2021). Instead, a strain gauge was attached to a column at the lower storey of each frame (S1 and S2) to measure the dynamic strain response along the longitudinal direction of the column. This has been considered a more direct seismic performance measure of the structure.

The acceleration time series recorded at the structural foundation by A3 and A10 can be integrated twice to obtain the displacement time series so that the amplification of horizontal foundation displacement can be inspected. Meanwhile, a pair of accelerometers were mounted on the edges of each frame (A4 and A5, A11 and A12) to measure the vertical acceleration, from which the vertical displacement can be computed as well. The foundation rotation can then be calculated and compared between the two models. The amplification of foundation responses is a feature of the first branch of GSI systems (Tsang and Pitilakis 2023), as an outcome of the augmented translational and rocking motions of the structural foundation.

On the other hand, two sets of sensors were installed to measure the responses of the foundation soils. A pair of accelerometers were placed at two depth levels below the structural foundation, one at the interface between the two HDPU sheets (A6) and the other at the interface between the bottom HDPU sheet and the underlying natural soil (A7). The sensors were also placed at the same depths in the reference model with natural soil immediately underneath of the structural foundation (A13 and A14). The shear stress-strain response of the two foundation materials can be calculated based on an approximation method proposed by Zeghal and Elgamal (1994).

Lastly, LVDT displacement sensors, L1 and L2, were set at the top of the frames to monitor the vertical movement, which was largely due to ground settlement. Two stages of settlement have been recorded. First, the movement was measured from the beginning of the flight until reaching the centrifugal acceleration of 50 g, which represents the immediate ground settlement due to the self-weight of the structure and the soil. The second stage was about the vertical movement during earthquake shaking to investigate the shaking-induced settlement. This information can provide valuable experimental data for checking the serviceability performance of the proposed system.

3.3 Input ground motions

The shaker in the centrifuge was used to replicate strong ground motions recorded in eight major earthquakes that were selected from the PEER NGA-West2 database (Ancheta et al. 2014). Table 1 provides a summary of the basic information of the selected ground motion records, including the unique record sequence number (RSN), with the moment magnitude of the earthquakes (M_w) ranging from 6.5 to 7.4 and peak ground acceleration (PGA) values of the original records ranging from 0.41 to 1.78 g.

All eight earthquake excitations were applied successively in each flight. Figure 4 displays the 5%-damped elastic acceleration response spectra for the eight input motions that were recorded at the base of the laminar box (A15 shown in Fig. 3) during the test for GSI Configuration C1. Distinctive frequency contents of the selected ground motion records can be observed. Thus, the study examined the robustness of the GSI-HDPU systems in terms of ground motions with different frequency contents. Note that different shaking levels for the same event were applied in the tests for the other two GSI configurations

Table 1 Overview of the earthquake ground motion records selected for the centrifuge testing

RSN	Event	Local date	M_w	Recording station	Recorded PGA (g)
77	San Fernando, US	9 February 1971	6.6	Pacoima Dam	1.22
139	Tabas, Iran	16 September 1978	7.4	Dayhook	0.32
160	Imperial Valley, US	15 October 1979	6.5	Bonds Corner	1.22
779	Loma Prieta, US	17 October 1989	6.9	LGPC	0.61
879	Landers, US	28 June 1992	7.3	Lucerne	0.73
1087	Northridge, US	17 January 1994	6.7	Tarzana	1.78
3968	Tottori, Japan	6 October 2000	6.7	TTRH02	0.77
4210	Niigata, Japan	23 October 2004	6.6	NIG020	0.41

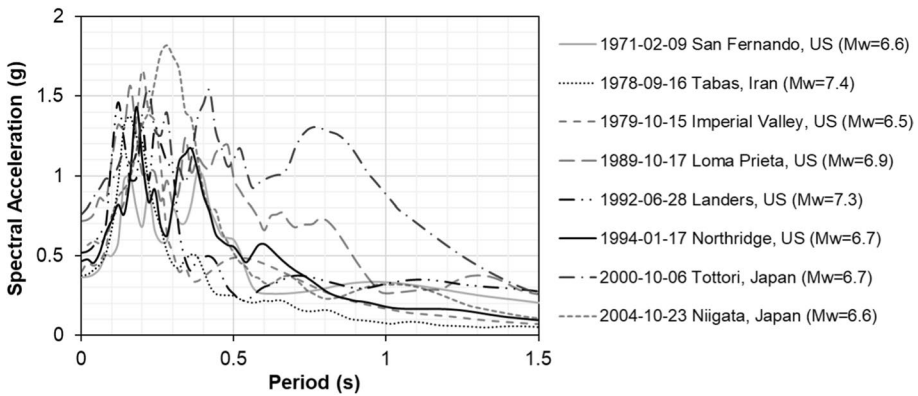


Fig. 4 5%-damped elastic acceleration response spectra of the earthquake ground motions applied at the base of the laminar box during the test for GSI Configuration C1

because it is known to be challenging to achieve exactly the same shaking level in different flights of centrifuge tests.

4 Results and discussion

4.1 Structural demand

4.1.1 Roof acceleration

Figure 5 shows the roof acceleration time series that was directly measured by the accelerometers, A1 and A8, in the test for GSI Configuration C1. The corresponding Fourier amplitude spectra are shown in Fig. 6. The response reduction and the change in frequency contents can be inspected qualitatively from the plots. Both the reduction of roof acceleration and the shift of the system’s natural frequency are significant in all earthquakes. The results for Configuration C2a and C4 are not shown, as their patterns were found to be similar to those for C1. In general, C2a shows lower response reductions, whilst C4 results

Table 2 Percentage reduction of the peak value and root-mean-square value (in parenthesis) of the total acceleration response recorded at the roof and the axial strain measured on a column at the lower storey of the frame with GSI system compared to the reference model with natural soil

Event	GSI-C1		GSI-C2a		GSI-C4	
	Acceleration	Strain	Acceleration	Strain	Acceleration	Strain
San Fernando, US	67 (76)	58 (68)	38 (46)	64 (56)	74 (81)	56 (72)
Tabas, Iran	74 (81)	69 (75)	40 (54)	61 (59)	85 (88)	70 (79)
Imperial Valley, US	55 (73)	55 (63)	36 (32)	31 (25)	56 (73)	53 (67)
Loma Prieta, US	41 (62)	61 (69)	35 (28)	22 (27)	55 (68)	57 (59)
Landers, US	69 (79)	75 (82)	33 (26)	49 (15)	70 (83)	70 (78)
Northridge, US	67 (79)	63 (73)	33 (41)	36 (38)	62 (84)	44 (74)
Tottori, Japan	35 (52)	31 (45)	30 (41)	30 (35)	68 (80)	58 (75)
Niigata, Japan	67 (79)	70 (73)	35 (34)	35 (27)	73 (80)	58 (75)
Average	59 (73)	61 (69)	35 (38)	41 (36)	68 (80)	58 (73)

in higher reductions. Moreover, the data recorded by the accelerometers at the floor level, A2 and A9, indicate very similar behaviour. This is reasonable given that the dynamic response of the test model is dominated by its first translational mode. The roof and the floor are expected to move in phase. Therefore, the results for the floor acceleration are also not shown.

Table 2 summarises the percentage reductions for all cases. The results show that the use of HDPU for C1 can reduce the peak acceleration demand by 35–74% (59% on average), whilst C2a and C4 can result in a demand reduction of 30–40% (35% on average) and 55–85% (68% on average) respectively. The reduction rates obtained from this study are generally higher than the average of 40–50% reduction obtained by Tsang et al. (2021) based on a 2-m layer of gravel-rubber mixtures, whereas the HDPU layer used in this study was only 0.6 m thick. Moreover, the percentage reductions of the root-mean-square values are given in parentheses in the table. For most cases, the percentage reduction of the root-mean-square value is greater than that of the peak value. A closer look at the results shows that the reduction rate is not sensitive to the shaking level.

4.1.2 Column strain

As a direct measure of the structural demand, the dynamic strain response along the longitudinal direction of a column at the lower storey of each frame has been recorded by the strain gauges (S1 and S2). It indicates the structural demand due mainly to the overturning moment of the frame, which is, in turn, a function of the roof and floor accelerations. However, there are other possible factors that contributed to the strain demand on the column. Therefore, the results of the column strain response are shown in this sub-section to confirm the isolation effectiveness of the proposed GSI-HDPU systems. The time series recorded in the test for GSI Configuration C1 are shown in Fig. 7 and the corresponding Fourier amplitude spectra are shown in Fig. 8. The reduction rates of both peak and root-mean-square strain values are included in Table 2.

Generally, the same trend can be observed between the two structural demand parameters and C2a also shows lower reductions in strain response. The GSI-C1 system can reduce the strain demand by 31–75% (61% on average), whilst a percentage reduction of

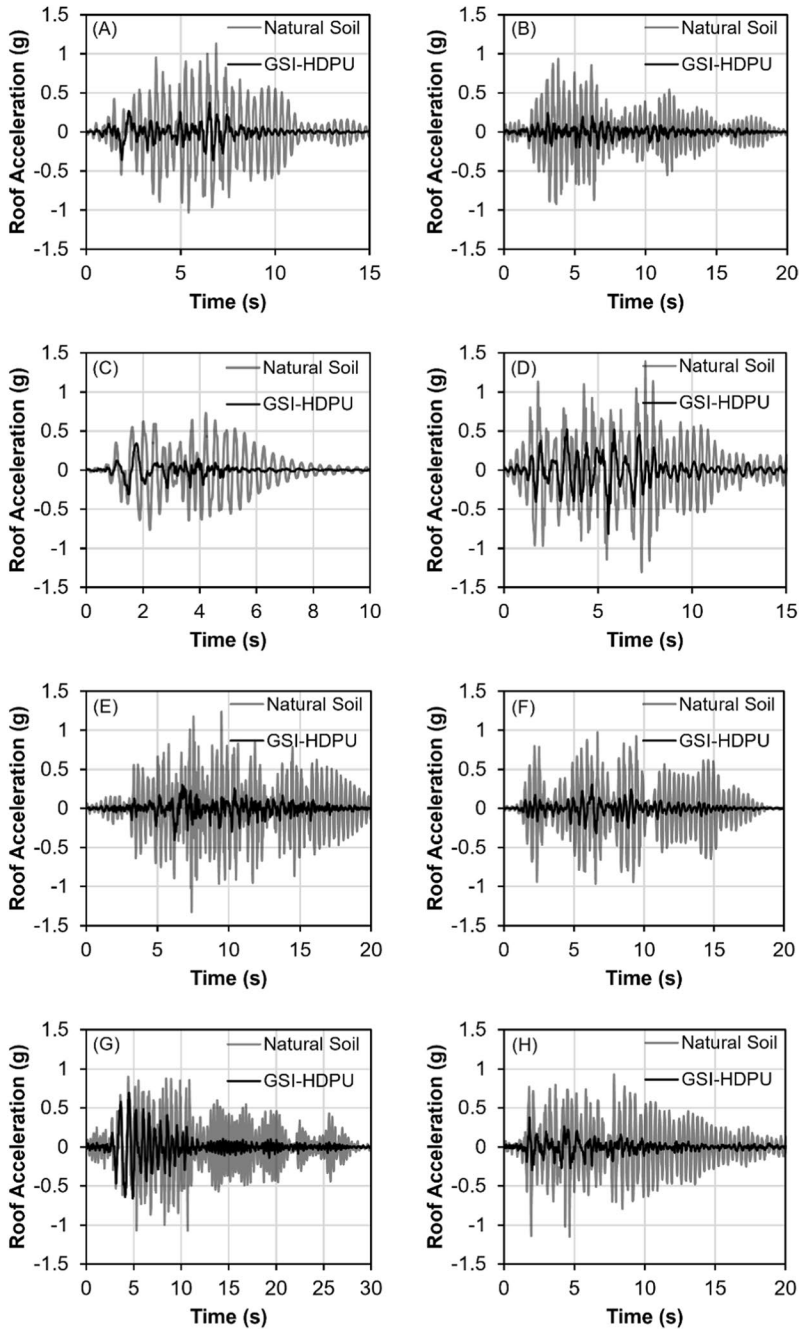


Fig. 5 Time series of the total acceleration response of GSI Configuration C1 based on HDPU recorded at the roof of the frame (in the prototype scale): **A** 1971 San Fernando earthquake; **B** 1978 Tabas earthquake; **C** 1979 Imperial Valley earthquake; **D** 1989 Loma Prieta earthquake; **E** 1992 Landers earthquake; **F** 1994 Northridge earthquake; **G** 2000 Tottori earthquake; and **H** 2004 Niigata earthquake

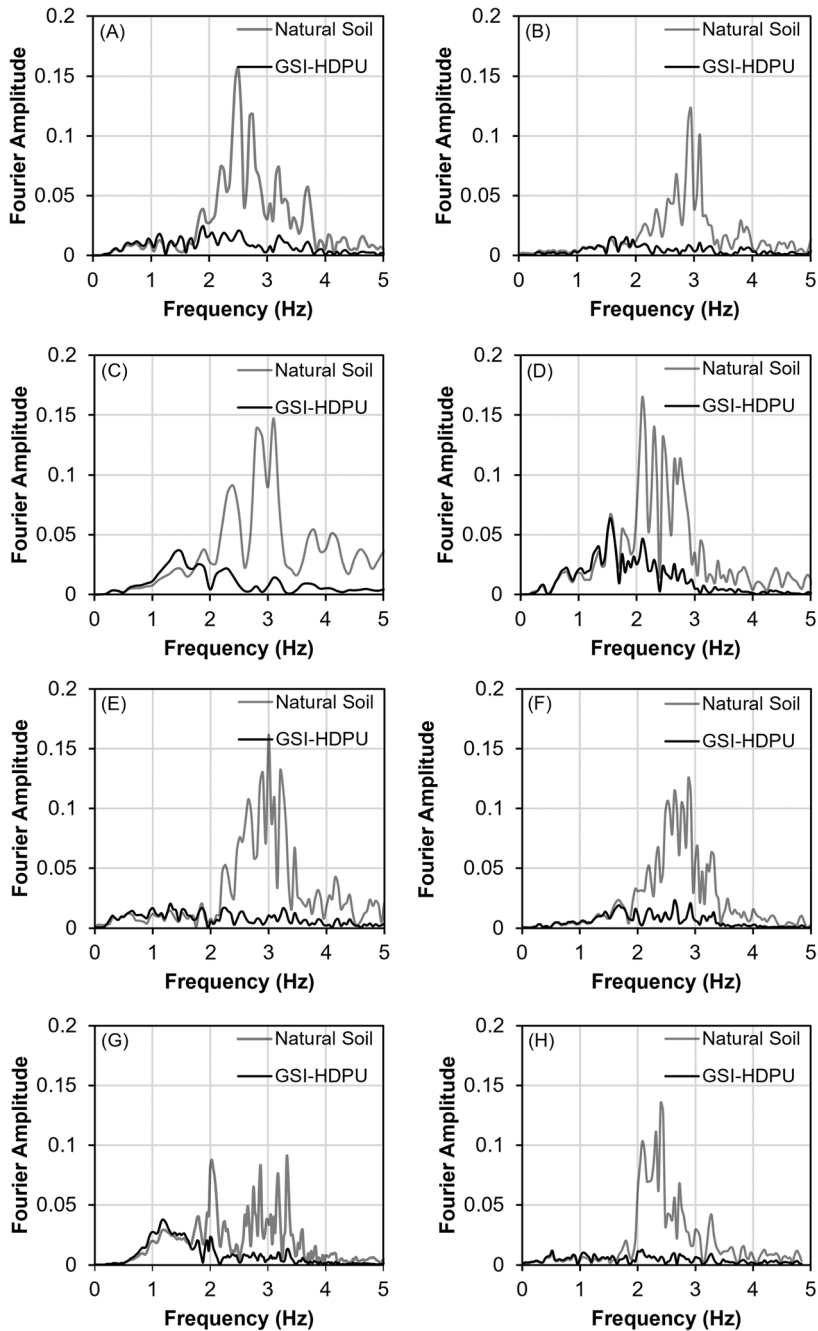


Fig. 6 Fourier amplitude spectra of the total acceleration response of GSI Configuration C1 based on HDPU recorded at the roof of the frame (in the prototype scale): **A** 1971 San Fernando earthquake; **B** 1978 Tabas earthquake; **C** 1979 Imperial Valley earthquake; **D** 1989 Loma Prieta earthquake; **E** 1992 Landers earthquake; **F** 1994 Northridge earthquake; **G** 2000 Tottori earthquake; and **H** 2004 Niigata earthquake

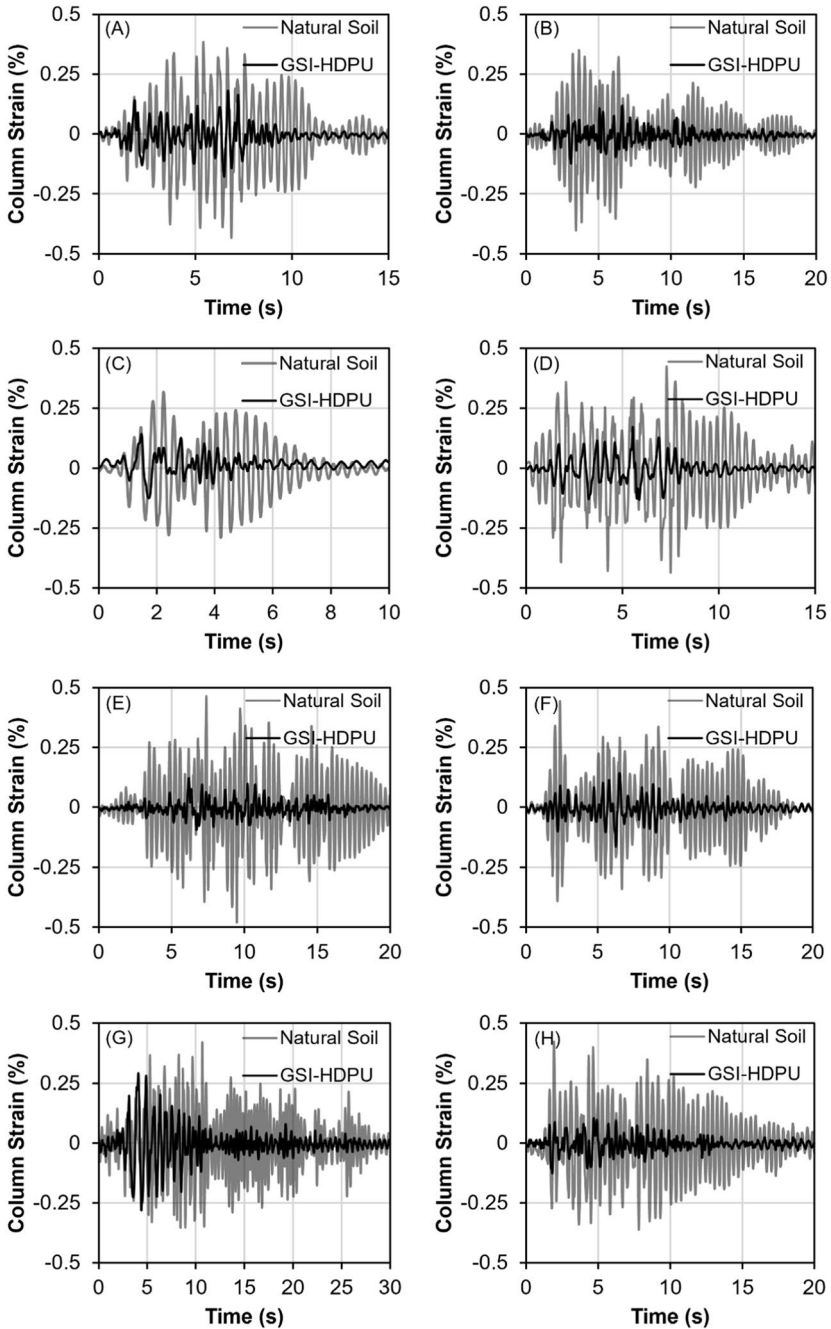


Fig. 7 Time series of the axial strain response of GSI Configuration C1 based on HDPU measured on a column at the lower storey of the frame: **A** 1971 San Fernando earthquake; **B** 1978 Tabas earthquake; **C** 1979 Imperial Valley earthquake; **D** 1989 Loma Prieta earthquake; **E** 1992 Landers earthquake; **F** 1994 Northridge earthquake; **G** 2000 Tottori earthquake; and **H** 2004 Niigata earthquake

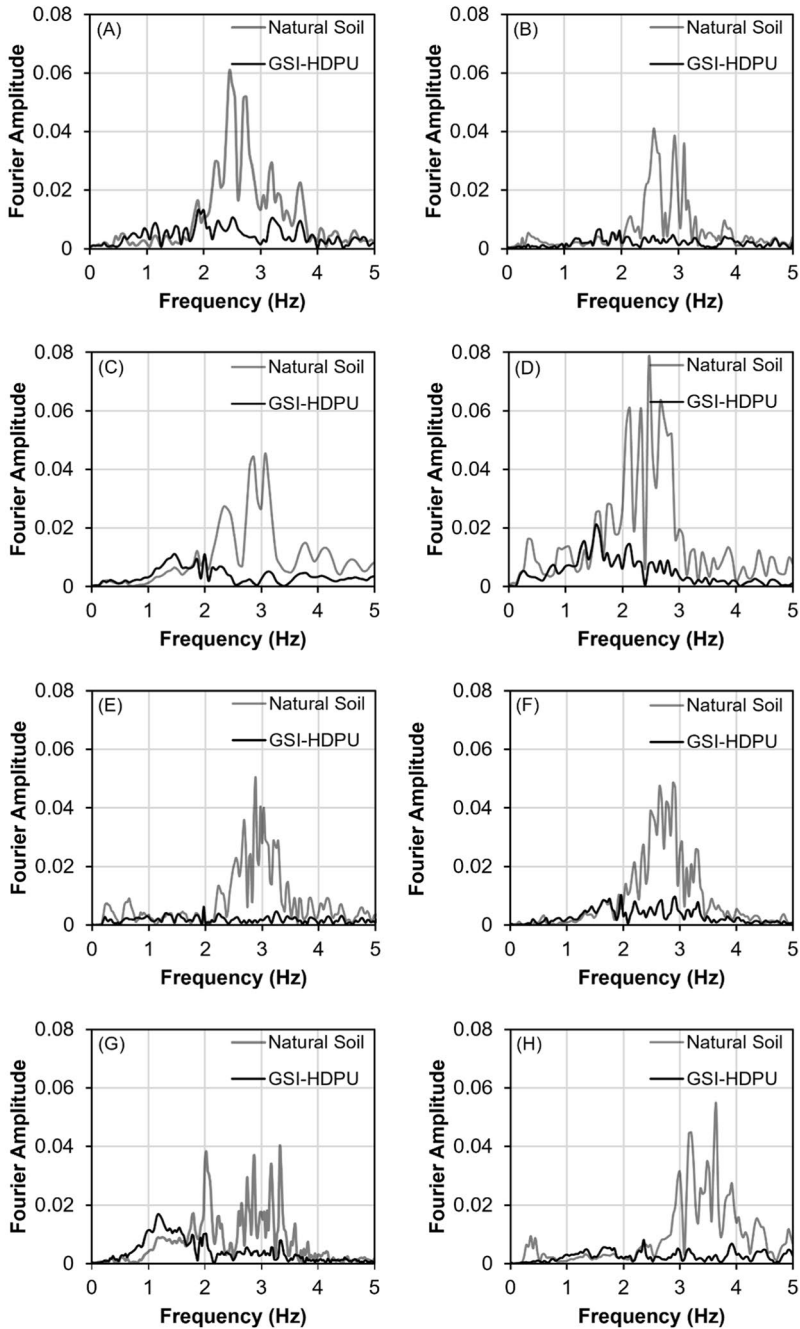


Fig. 8 Fourier amplitude spectra of the axial strain response of GSI Configuration C1 based on HDPU measured on a column at the lower storey of the frame: **A** 1971 San Fernando earthquake; **B** 1978 Tabas earthquake; **C** 1979 Imperial Valley earthquake; **D** 1989 Loma Prieta earthquake; **E** 1992 Landers earthquake; **F** 1994 Northridge earthquake; **G** 2000 Tottori earthquake; and **H** 2004 Niigata earthquake

22–64% (41% on average) and 44–70% (58% on average) can be observed for C2a and C4 respectively. The percentage reduction of the root-mean-square value is greater than that of the peak value for most cases.

4.1.3 Fundamental natural frequency

The GSI systems investigated in this study facilitate the beneficial effects of dynamic soil-foundation-structure interaction. The reduction of structural demand partly resulted from the shifting of the system’s natural period. Therefore, it is meaningful to inspect the changes in the natural period/frequency of the systems.

Firstly, a single cycle of a sinusoidal wave of 1 Hz was applied before the earthquake events were employed. The wave had a low amplitude of around 0.01 g. The acceleration responses at the roof of the two frame models were recorded and the corresponding Fourier amplitude spectra were computed. The predominant frequency of the acceleration response identified for each model is summarised in Table 3. Compared to the fundamental natural frequency of 3.5 Hz of the fixed-base frame, the fundamental natural frequencies of all the soil-foundation-structure systems have been decreased. The fundamental natural period was lengthened by 12% for natural soil, 84% for GSI-C1, 35% for GSI-C2a and 192% for GSI-C4. It is noteworthy that the fundamental natural frequencies of the three non-isolated systems with natural soil were very close to each other. This may indicate that the foundation soil was compacted in a consistent manner, with a comparable level of mechanical energy being applied.

Table 3 also summarises the fundamental natural frequencies of the two soil-foundation-structure systems during the eight earthquakes in each test based on the Fourier amplitude spectra of the acceleration response presented in Fig. 6 and their corresponding spectral ratio with respect to the applied motions at the base. The average values of the fundamental natural frequencies and the period-lengthening ratios of the GSI systems as compared to the model with natural soil were calculated. It is seen that the natural period of the GSI-HDPU systems has been increased by an average of 91% for

Table 3 Fundamental natural frequencies of the soil–foundation–structure systems based on the Fourier amplitude spectra of the acceleration response recorded during the low-amplitude shaking and the eight earthquakes in each test

	C1		C2a		C4	
	Natural Soil	GSI	Natural Soil	GSI	Natural Soil	GSI
Low-amplitude wave	3.1	1.9	3.2	2.6	3.1	1.2
San Fernando, US	2.7	1.5	3.0	2.4	2.8	1.0
Tabas, Iran	2.8	1.7	3.1	2.5	2.8	1.0
Imperial Valley, US	2.9	1.4	3.1	2.6	3.0	1.1
Loma Prieta, US	2.9	1.5	3.0	2.5	2.9	1.2
Landers, US	2.9	1.4	2.9	2.6	2.9	1.0
Northridge, US	2.8	1.5	2.9	2.4	2.9	1.1
Tottori, Japan	2.9	1.5	2.8	2.5	2.9	1.0
Niigata, Japan	2.9	1.5	2.9	2.3	2.9	1.2
Average	2.8	1.5	3.0	2.5	2.9	1.1

C1, 21% for C2a and 168% for C4. A clear correlation between the period-lengthening ratio and the demand reduction percentage can be observed amongst the three GSI configurations.

Moreover, the strong earthquake shaking induced nonlinear response of the foundation soil materials, which would reduce the stiffness of the foundation layer and further lengthen the system’s natural period. It is found that the GSI-C2a and GSI-C4 systems, as well as the non-isolated system, have undergone a period shift of around 5–10% during shaking. Meanwhile, an over 20% shift was observed in the GSI-C1 system, which had the largest interface area with HDPU amongst the three GSI configurations. The GSI-C4 system arguably had a large interface area with HDPU as well, but the introduction of lateral disconnection has already significantly reduced both the horizontal and rocking stiffnesses of the foundation system. As the effect of lateral disconnection is rather independent of the shaking level (Somma et al. 2022), the system’s natural period was therefore not much elongated further during shaking.

4.2 Foundation response

4.2.1 Base shear versus horizontal displacement

Figure 9 shows the base shear force versus horizontal displacement response of the foundation slab during the 1994 Northridge earthquake calculated for each GSI system. Similar behaviour can be observed in other earthquake events. The base shear force demand on the structure, V_b , calculated based on Eq. (1), was substantially lower for Configurations C1 and C4 compared to the non-isolated structure, whilst C2a exhibits a smaller reduction. The increase in the horizontal displacement of the foundation slab for C1 and C4 is analogous to the large shear deformation of laminated rubber bearings used for traditional ‘structural’ seismic isolation. It is important to keep this displacement within an acceptable limit in real applications.

$$V_b = -m_1\ddot{x}_1^T - m_2\ddot{x}_2^T \tag{1}$$

Noted that \ddot{x}_1^T and \ddot{x}_2^T are respectively the recorded acceleration response at the floor (measured by A2 and A9) and the roof (measured by A1 and A8). m_1 and m_2 are respectively the mass of the floor and the roof.

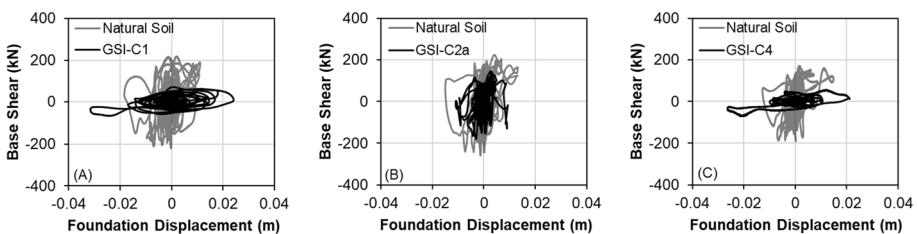


Fig. 9 Base shear force-horizontal displacement response of the foundation slab of each GSI configuration during the 1994 Northridge earthquake: **A** Configuration C1; **B** Configuration C2a; **C** Configuration C4

4.2.2 Base moment versus rotation

Figure 10 shows the base moment versus rotation response of the foundation slab during the 1994 Northridge earthquake calculated for each GSI system. Similar behaviour can also be observed in other events. As for the base shear force, the base moment demand on the structure, M_b , calculated based on Eq. (2), was also substantially lower for Configurations C1 and C4, whilst it was moderately reduced for C2a. It is noteworthy that the maximum rotation of the foundation slab, θ_f , of the GSI-C1 system was comparable to that of the non-isolated structure, even though the rocking stiffness of the foundation system was significantly reduced. Meanwhile, the maximum rotation was larger for C4 likely because of the lower rocking stiffness due to the introduction of lateral disconnection. The increase in foundation rotation is similar to that observed for rocking isolation (below the foundation). The lower rocking stiffness of C4 results in lower structural demand, as reported in the previous sub-section. In practice, the increased rotation needs to be checked against code limits to ensure structural integrity.

$$M_b = -m_1 \ddot{x}_1^T h_1 - m_2 \ddot{x}_2^T h_2 + m_1 g(x_1 + h_1 \theta_f) + m_2 g(x_2 + h_2 \theta_f) \tag{2}$$

Noted that h_1 and h_2 are respectively the height of the floor and the roof measured from the base of the footing foundation. x_1 and x_2 are respectively the horizontal displacement of the floor and the roof relative to the centre of the foundation. Lastly, g is the gravitational acceleration.

The threshold static base moment at the onset of uplift, M_{uplift} , estimated by using Eq. (3) following FEMA 274 (1997) is indicated by the solid horizontal lines on the plots in Fig. 10. It is observed that uplift might have occurred for the non-isolated structures during the 1994 Northridge earthquake, whilst the base moment of C1 and C4 was significantly reduced to the levels well below the threshold and that of the GSI-C2a system was reduced to somewhere close to the threshold. Similar results have been found in other earthquake events. This represents a potential benefit of using GSI systems that uplift can be prevented.

$$M_{uplift} = \frac{WL}{6} \tag{3}$$

Noted that W is the total weight of the model frame structure and L is the width of the foundation slab.

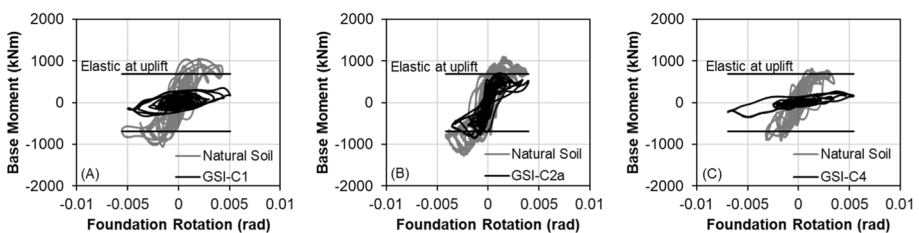


Fig. 10 Base moment-rotation response of the foundation slab of each GSI configuration during the 1994 Northridge earthquake: **A** Configuration C1; **B** Configuration C2a; **C** Configuration C4

4.2.3 Material hysteresis

Apart from the response of the foundation slab, the time-varying shear stress τ and shear strain γ at any depth z measured from the bottom of the raft foundation can be computed using the approximation method proposed by Zeghal and Elgamal (1994). Equations (4) and (5) were derived for calculating the shear stress at the mid-depth of the HDPU layer, $z = d_s/2$, underneath the raft foundation and the shear strain averaged across the HDPU layer at time t . The shear stress and strain responses of the natural soil in the reference cases were also calculated at the same depth for a direct comparison.

$$\tau\left(\frac{d_s}{2}, t\right) = \rho d_s \frac{\ddot{u}\left(\frac{d_s}{2}, t\right) + \ddot{u}(0, t)}{4} \tag{4}$$

$$\gamma(t) = \frac{u(d_s, t) - u(0, t)}{d_s} \tag{5}$$

where ρ is the mass density of the foundation material, u and \ddot{u} are the horizontal displacement and acceleration response respectively. A band-pass filter over the frequency range from 0.2 to 20 Hz (in the prototype scale) was applied to the acceleration data before integrating with respect to time twice to obtain the displacement (Kutter et al. 2018).

Since the acceleration at the ground surface, as required in Eq. (4), can rarely be measured in centrifuge testing, Brennan et al. (2005) recommended a linear fit between the top pair of accelerometers (A6 and A7, A13 and A14), from which the linear relationship of the acceleration responses can be extrapolated to the ground surface. The horizontal displacement response of the foundation slab was taken as the displacement at $z=0$, as required in Eq. (5). Figure 11 shows the full shear stress-strain history at the mid-depth of the HDPU layer and at the same depth for the natural soil layer in the non-isolated cases using the measurements from the 1994 Northridge earthquake as an illustration.

The HDPU material is shown to be much softer than the natural soil, as expected. The shear stress-strain response of the HDPU material exhibits high hysteretic damping. In comparison with the hysteresis of rubber-soil mixtures previously reported by the project team in Tsang et al. (2021), the HDPU material produced wider hysteretic loops that indicate even higher energy absorption capability. This is an advantage of using HDPU material for creating GSI systems. Hence, the high-damping property of the HDPU material, along with its other characteristics, has confirmed its suitability for protecting

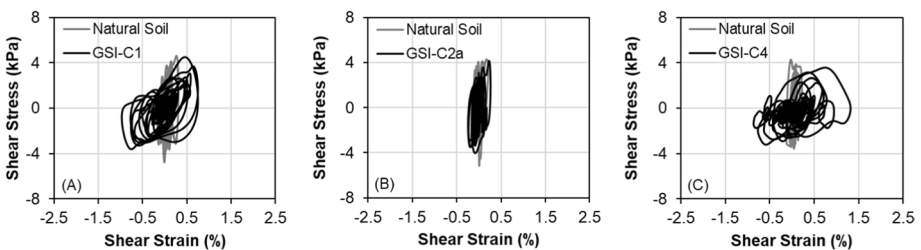


Fig. 11 Shear stress-strain response of the HDPU foundation materials of each GSI configuration during the 1994 Northridge earthquake: **A** Configuration C1; **B** Configuration C2a; **C** Configuration C4

acceleration-sensitive structures and equipment. Noted that different shapes of the hysteresis can be observed in other earthquake events, but the general behaviours are similar.

4.2.4 Ground settlement

On the other hand, the vertical movement of the frame structure was monitored by the LVDT displacement sensors, L1 and L2. This can inform the amount of ground settlement (reported in the prototype scale below) that was induced (1) when the centrifugal acceleration increased gradually up to the target level of 50 g and (2) during the earthquake shaking. The immediate settlement due to the self-weight of the frame sitting on natural soil was consistently around 3 mm, whereas the immediate settlement of the three GSI systems was 11.5 mm, 2.5 mm and 9.8 mm, respectively, for C1, C2a and C4, which is not excessive with respect to the serviceability requirements stipulated in design codes and standards. For the GSI-C1 system with the 0.6 m thick HDPU layer, the amount of immediate ground settlement is comparable to that based on the use of 2–3 m thick rubber-soil mixtures estimated via numerical and analytical approaches as reported in Tsang et al. (2023). This is considered reasonable given the lower modulus of the HDPU materials. The movement of Configuration C2a was expected to be comparable to the non-isolated counterpart because the frame was also sitting on NS. For GSI configurations C1 and C4, the deformation was 7–9 mm larger due to the softness of HDPU, which is merely 1–1.5% of the 600 mm thick HDPU layer in the prototype scale. More importantly, given the homogenous and robust mechanical properties of the manufactured HDPU sheets, the movement is expected to be uniform across the entire foundation.

Given the known properties of HDPU materials, the amount of deformation can be predicted and taken into account in the design process. A key parameter for estimating ground settlement is the small-strain shear modulus. Based on the low-amplitude sinusoidal wave that was applied to the model, the time difference between the first peaks of the motions recorded by two adjacent accelerometers (A6 and A7 for GSI, A13 and A14 for natural soil) after low-pass filtering with a cut-off frequency of 20 Hz can be calculated. With a distance of 0.3 m (in the prototype scale) between the two accelerometers, the shear wave velocity has been found to be 203 and 48 m/s, respectively, for natural soil and HDPU. The corresponding small-strain shear modulus would be 66 and 2.9 MPa respectively. With these values, the hand-calculation approaches evaluated in Tsang et al. (2023) can be used for estimating the immediate ground settlement.

On the other hand, the vertical movements of the foundation slab during the eight earthquakes were monitored to investigate the shaking-induced ground settlement. Figure 12 shows the recordings taken during the 1994 Northridge earthquake. It is seen that the vertical movement fluctuated and generally increased when the shaking was more intense. When the frame structure was sitting on natural soil, including the GSI-C2a system, the final ground settlement was around 10 mm, which was very consistent amongst different tests. Meanwhile, it is found that the final ground settlement was around 6–7 mm when the structure was sitting on HDPU sheets. In other words, the use of the GSI-C1 or GSI-C4 system can reduce the shaking-induced ground settlement, which is an additional benefit of using GSI-HDPU systems. This is because the HDPU material adopted in this study was in the form of a uniform, homogenous solid, no packing of particles would occur during shaking. Despite the high deformability of the HDPU materials, most of the deformations had already occurred due to the self-weight of the structure.

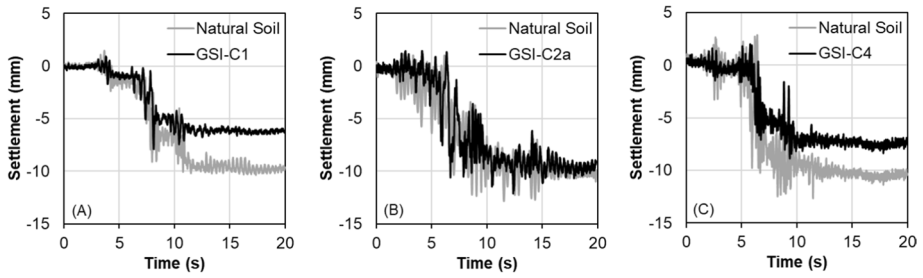


Fig. 12 Time series of the ground settlement of the foundation slab of each GSI configuration during the 1994 Northridge earthquake: **A** Configuration C1; **B** Configuration C2a; **C** Configuration C4

4.3 Foundation stiffness

4.3.1 Horizontal stiffness

From the hysteretic loops of the base shear force against the horizontal displacement of the foundation slab as shown in Fig. 9, the horizontal stiffness of the foundation system can be calculated for each loop, which is related with the average displacement amplitude of the peak positive and peak negative values of the loop, because the loops are typically not symmetric about the origin. Figure 13 shows the relationships between the horizontal stiffness versus the average displacement amplitude for each GSI configuration, taking the measurements from the 1994 Northridge earthquake as an example. A trendline using an exponential function is shown for each set of data to assist in making comparison.

In general, the horizontal stiffness of the GSI-C1 and GSI-C4 systems are significantly lower than that of the non-isolated system (i.e., natural soil). The difference is in the order of 10 times, which reflects the low modulus value of the HDPU material adopted in this study. A closer inspection would inform that the horizontal stiffness of C4 appears to be slightly lower than that of C1, which should be reasonable given the introduction of lateral disconnection in C4 as opposed to the use of HDPU surrounding the entire foundation system in C1. On the other hand, the horizontal stiffness of the GSI-C2a system is shown to be very close to that of the non-isolated system, especially at low displacement amplitudes. When the displacement amplitude increased, the horizontal stiffness was reduced, due to the nonlinearity of the HDPU materials at the periphery of the foundation system. The

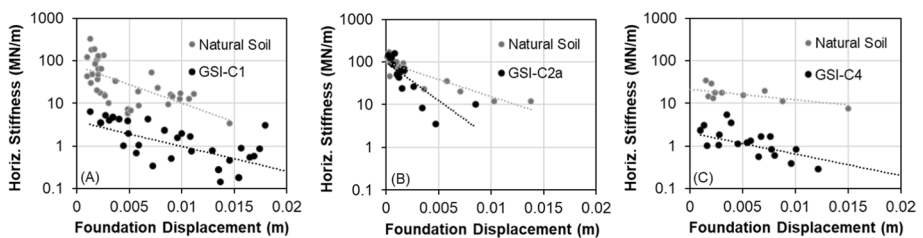


Fig. 13 Horizontal stiffness versus displacement amplitude of the foundation system of each GSI configuration during the 1994 Northridge earthquake: **A** Configuration C1; **B** Configuration C2a; **C** Configuration C4

result also seems to indicate that the foundation material underneath the raft footing has a more dominant effect on the horizontal stiffness than the material at the periphery, which can probably be explained by the larger contact area at the footing base compared to the sides of the footing.

4.3.2 Rocking stiffness

Likewise, the rocking stiffness of the foundation system can be calculated for each loop of the base moment against the rotation of the foundation slab as shown in Fig. 10. Figure 14 shows the relationships between the rocking stiffness versus the average rotation amplitude of the peak positive and peak negative values for each GSI configuration, taking the measurements from the 1994 Northridge earthquake as an example. A trendline using an exponential function is also shown for each set of data for comparison.

The GSI-C1 and GSI-C4 systems exhibit significantly lower rocking stiffness than that of the non-isolated system. The difference is more than 10 times at smaller rotation amplitudes, whilst the difference becomes smaller at larger rotation amplitudes. It can also be seen that the rocking stiffness of C4 is slightly lower than that of C1 due to the use of lateral disconnection in C4. Comparing the rocking stiffness of the GSI-C2a system and the non-isolated system, the difference is even smaller than that in the horizontal stiffness. This is because the foundation materials underneath the raft footing are essentially the same. This supports the notion that the foundation material underneath the raft footing has a more dominant effect than the material at the periphery on the stiffnesses of the foundation system especially on the rocking stiffness. This has an important implication for the design of the first branch of GSI systems, which is based on facilitating the beneficial effects of dynamic soil-foundation-structure interaction.

4.3.3 Backbone curves

Based on the horizontal stiffness-displacement and rocking stiffness-rotation correlations, the theoretical base shear-horizontal displacement and base moment-rotation backbone curves for the three GSI-HDPU systems can be plotted in Fig. 15 for direct comparison. Noted that a factor of two has been applied when calculating all the stiffness values to capture the variability of data in Figs. 13 and 14. It is clear that the base shear and moment demand can be significantly reduced in the GSI-C1 and GSI-C4 systems. An important observation is that for the reference (non-isolated) case and the GSI-C2a system, the peak base shear and moment are reached at a smaller displacement/rotation response, whilst

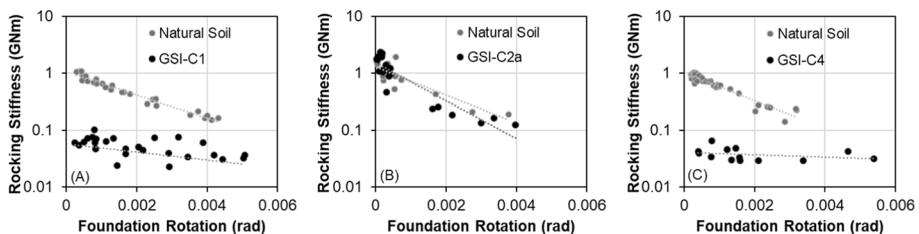


Fig. 14 Rocking stiffness versus rotation amplitude of the foundation system of each GSI configuration during the 1994 Northridge earthquake: **A** Configuration C1; **B** Configuration C2a; **C** Configuration C4

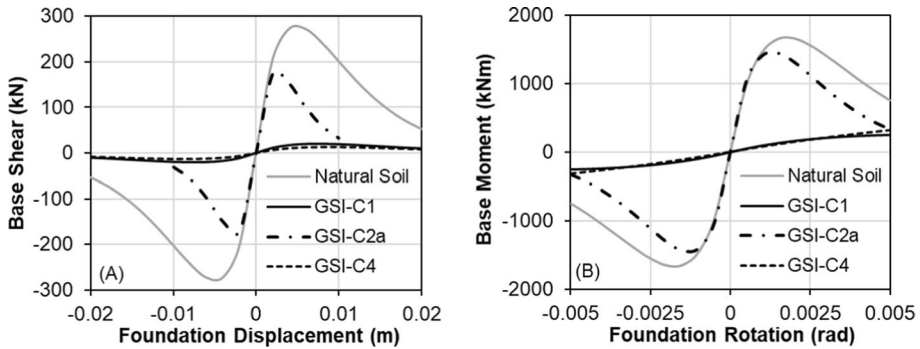


Fig. 15 Backbone curves of the **A** base shear-horizontal displacement response and **B** base moment-rotation response of the foundation slab for the three GSI-HDPU systems and the (reference) non-isolated system

they peak at a larger displacement/rotation response for C1 and C4. This indicates a more deformable foundation system that can avoid undesirable soil failure. This is another advantage of the use of HDPU materials for creating GSI systems.

5 Conclusions

A thin and homogeneous layer of high-damping polyurethane (HDPU) is proposed to be used for realising geotechnical seismic isolation (GSI) in this article. The dynamic response behaviour and isolation performance of three configurations of GSI-HDPU systems were investigated via centrifuge testing. It was found that the proposed systems can effectively reduce the structural demand, in terms of the roof acceleration and column strain, by an average of 60–70% with HDPU around the entire foundation (C1), 35–40% with HDPU around the periphery of the foundation only (C2a), and 60–80% with HDPU underneath the foundation only in addition to the introduction of lateral disconnection (C4).

The mechanism of GSI-HDPU systems is based on facilitating the beneficial effects of dynamic soil-foundation-structure interaction, such that structural demand can be reduced from the shifting of the system's natural period. Therefore, the changes in the natural period/frequency of the system were inspected. It was observed from the centrifuge tests that the fundamental natural period has been increased by an average of 91% for C1, 21% for C2a and 168% for C4, which clearly correlate with the demand reduction rates. Meanwhile, HDPU material possesses high-damping properties, rendering its suitability as a GSI foundation material for protecting acceleration-sensitive structures and equipment.

On the other hand, a closer inspection revealed that the horizontal and rocking stiffnesses of the GSI-C1 and GSI-C4 systems were significantly lower than those of the non-isolated system and they reduced further as the foundation displacement and rotation amplitudes increased. As a result, the horizontal displacement responses of the foundation slab were increased, which is analogous to the large shear deformation of laminated rubber bearings in traditional 'structural' seismic isolation. It is, however, interesting to see comparable rotation responses of the foundation slab between the GSI-C1 system and the non-isolated structure, which is beneficial as it reduces the likelihood of foundation uplift.

Another benefit of using HDPU is the small thickness required for creating effective GSI systems. Despite the softness of the HDPU material, the immediate ground settlement due to the self-weight of the structure and the soil was found to be well below the serviceability limits stipulated in design codes and standards. It is also noteworthy that the vertical movement is expected to be uniform across the entire foundation due to the homogenous and robust mechanical properties of the manufactured HDPU sheets. The small-strain shear modulus of the HDPU materials used in this study was estimated based on the test data, which can be employed for predicting ground settlement as well.

In closing, the proposed group of GSI-HDPU systems has been proved to be effective in reducing seismic demand, and hence, enhancing the resilience of structures, minimising material and energy consumptions and reducing the embodied carbon footprints of new constructions. Amongst the three GSI configurations investigated in this study, one of them is a non-invasive technique that is suitable for retrofitting existing structures. This can help conserve heritage structures, prolong the life of our building stock and reduce demolition waste. GSI is a sustainable construction method, which can reduce the negative health and environmental impacts caused by construction and the built-up environment.

Funding Open Access funding enabled and organized by CAUL and its Member Institutions. This study is a part of the PhD project conducted by the second author who is financially supported by the Swinburne University Postgraduate Research Award.

Data availability The datasets generated during and/or analysed during the current study are available from the author on reasonable request.

Declarations

Conflict of interest The author has no relevant financial or non-financial interests to disclose.

Open Access This article is licensed under a Creative Commons Attribution 4.0 International License, which permits use, sharing, adaptation, distribution and reproduction in any medium or format, as long as you give appropriate credit to the original author(s) and the source, provide a link to the Creative Commons licence, and indicate if changes were made. The images or other third party material in this article are included in the article's Creative Commons licence, unless indicated otherwise in a credit line to the material. If material is not included in the article's Creative Commons licence and your intended use is not permitted by statutory regulation or exceeds the permitted use, you will need to obtain permission directly from the copyright holder. To view a copy of this licence, visit <http://creativecommons.org/licenses/by/4.0/>.

References

- Akhtar AY, Tsang HH (2023) Dynamic properties of recycled polyurethane-coated rubber-soil mixtures. *Case Stud Constr Mater* 18:e01859
- Aloisio A, Contento A, Xue J, Fu R, Fragiaco M, Briseghella B (2023) Probabilistic formulation for the q-factor of piles with damping pre-hole. *Bull Earthq Eng* 21(8):3749–3775
- Ancheta TD, Darragh RB, Stewart JP, Seyhan E, Silva WJ, Chiou BSJ, Wooddell KE, Graves RW, Kottke AR, Boore DM, Kishida T, Donahue JL (2014) NGA-West2 database. *Earthq Spectra* 30(3):989–1005
- ASTM D4253-16e1. Standard test methods for Maximum Index Density and Unit Weight of soils using a vibratory table. ASTM International, West Conshohocken, PA, USA
- ASTM D4254-16. Standard test methods for Minimum Index Density and Unit Weight of soils and calculation of relative density. ASTM International, West Conshohocken, PA, USA

- ASTM D792-20. Standard test methods for density and specific gravity (relative density) of plastics by displacement. ASTM International, West Conshohocken, PA, USA
- ASTM D854-14. Standard test methods for specific gravity of soil solids by Water Pycnometer. ASTM International, West Conshohocken, PA, USA
- Banović I, Radnić J, Grgić N, Semren K (2023) Effectiveness of several low-cost geotechnical seismic isolation methods: a shake-table study. *Bull Earthq Eng* 21(8):3923–3947
- Bernal-Sanchez J, Leak J, Barreto D (2023) Rubber–soil mixtures: use of grading entropy theory to evaluate stiffness and liquefaction susceptibility. *Bull Earthq Eng* 21(8):3777–3796
- Brennan AJ, Thusyanthan NI, Madabhushi SPG (2005) Evaluation of shear modulus and damping in dynamic centrifuge tests. *J Geotech Geoenviron Eng* 131(12):1488–1497
- Brunet S, De la Llera JC, Kausel E (2016) Non-linear modeling of seismic isolation systems made of recycled tire-rubber. *Soil Dyn Earthq Eng* 85:134–145
- Chiaro G, Palermo A, Banasiak L, Tasalloti A, Granello G, Hernandez E (2023) Seismic response of low-rise buildings with eco-rubber geotechnical seismic isolation (ERGSi) foundation system: numerical investigation. *Bull Earthq Eng* 21(8):3797–3821
- Dhanya JS, Fouzul MA, Banerjee S, Boominathan A, Zhussupbekov A (2023) Shaking table experiments on framed structure resting on geogrid reinforced geotechnical seismic isolation system. *Bull Earthq Eng* 21(8):3823–3849
- Edinçliler A, Yıldız Ö (2023) Shaking table tests on geotechnical seismic isolation for medium-rise buildings using EPS beads-sand mixtures. *Bull Earthq Eng* 21(8):3851–3877
- FEMA 274 (1997) NEHRP guidelines for the seismic rehabilitation of buildings. Prepared for the building seismic safety council. Federal Emergency Management Agency, Washington, D.C
- Forcellini D, Alzabeebe S (2023) Seismic fragility assessment of geotechnical seismic isolation (GSI) for bridge configuration. *Bull Earthq Eng* 21(8):3969–3990
- Garnier J, Gaudin C, Springman SM, Culligan PJ, Goodings DJ, König D et al (2007) Catalogue of scaling laws and similitude questions in geotechnical centrifuge modelling. *Int J Phys Model Geotech* 8(3):1–23
- Gatto MPA, Lentini V, Montrasio L (2023) Dynamic properties of polyurethane from resonant column tests for numerical GSI study. *Bull Earthq Eng* 21(8):3991–4017
- Karatzia X, Mylonakis G (2017) Geotechnical isolation of pile-supported bridge piers using EPS geo-foam. In: Proceedings of the 16th world conference on earthquake engineering, Santiago, Chile
- Kirtas E, Rovithis E, Ptilakis K (2009) Subsoil interventions effect on structural seismic response. Part I: validation of numerical simulations. *J Earthq Eng* 13(2):155–169
- Kutter B, Carey T, Hashimoto T, Zeghal M, Abdoun T, Kokalli P, Madabhushi G, Haigh S, Hung W-Y, Lee C-J, Iai S, Tobita T, Zhou YG, Chen Y, Manzari MT (2018) LEAP-GWU-2015 experiment specifications, results, and comparisons. *Soil Dyn Earthq Eng* 113:616–628
- Lee C-J, Hung W-Y, Tsai C-H, Chen T, Tu Y, Huang C-C (2014) Shear wave velocity measurements and soil–pile system identifications in dynamic centrifuge tests. *Bull Earthq Eng* 12:717–734
- Nikitas G, Bhattacharya S (2023) Experimental study on sand–tire chip mixture foundations acting as a soil liquefaction countermeasure. *Bull Earthq Eng* 21(8):4037–4063
- Ptilakis K, Karapetrou S, Tsagdi K (2015) Numerical investigation of the seismic response of RC buildings on soil replaced with rubber–sand mixtures. *Soil Dyn Earthq Eng* 79:237–252
- Shimamura A (2012) Study on earthquake response reduction by improved composite geo-material using rubber chips and fibrous materials (translated from Japanese). PhD Thesis, Osaka University, Japan
- Somma F, Flora A (2023) SAP–sand mixtures as a geotechnical seismic isolation technology: from the dynamic characterization to a simple analytical design approach. *Bull Earthq Eng* 21(8):4065–4089
- Somma F, Bilotta E, Flora A, Viggiani GMB (2022) Centrifuge modeling of shallow foundation lateral disconnection to reduce seismic vulnerability. *J Geotech Geoenviron Eng (ASCE)* 148(2):04021187
- Tsang HH (2008) Seismic isolation by rubber–soil mixtures for developing countries. *Earthq Eng Struct Dyn* 37(2):283–303
- Tsang HH (2009) Geotechnical seismic isolation. *Earthquake engineering: new research*. Nova Science Publishers Inc, New York, pp 55–87
- Tsang HH (2023) Analytical design models for geotechnical seismic isolation systems. *Bull Earthq Eng* 21(8):3881–3904
- Tsang HH, Ptilakis K (2019) Mechanism of geotechnical seismic isolation system: analytical modeling. *Soil Dyn Earthq Eng* 122:171–184
- Tsang HH, Ptilakis K (2023) Preface for the special issue on geotechnical seismic isolation (GSI). *Bull Earthq Eng* 21(8):3745–3748
- Tsang HH, Lo SH, Xu X, Sheikh MN (2012) Seismic isolation for low-to-medium-rise buildings using granulated rubber–soil mixtures: numerical study. *Earthq Eng Struct Dyn* 41:2009–2024

- Tsang HH, Tran DP, Hung WY, Pitilakis K, Gad EF (2021) Performance of geotechnical seismic isolation system using rubber–soil mixtures in centrifuge testing. *Earthq Eng Struct Dyn* 50(5):1271–1289
- Tsang HH, Tran DP, Gad EF (2023) Serviceability performance of buildings founded on rubber-soil mixtures for geotechnical seismic isolation. *Aust J Struct Eng* 24(4):265–278
- Vratsikidis A, Pitilakis D (2023) Field testing of gravel–rubber mixtures as geotechnical seismic isolation. *Bull Earthq Eng* 21(8):3905–3922
- Yegian MK, Kadakal U (2004) Foundation isolation for seismic protection using a smooth synthetic liner. *J Geotech Geoenviron Eng (ASCE)* 130(11):1121–1130
- Yuan K, Gan D, Guo J, Xu W (2021) Hybrid geotechnical and structural seismic isolation: shake table tests. *Earthq Eng Struct Dyn* 50:3184–3200
- Zeghal M, Elgamal A-W (1994) Analysis of site liquefaction using Earthquake records. *J Geotech Eng* 120(6):996–1017

Publisher's Note Springer Nature remains neutral with regard to jurisdictional claims in published maps and institutional affiliations.